DOI: 10.1002/chem.200701099

Modeling the Photochemistry of the Reference Phototoxic Drug Lomefloxacin by Steady-State and Time-Resolved Experiments, and DFT and Post-HF Calculations

Mauro Freccero,*[a] Elisa Fasani,[a] Mariella Mella,[a] Ilse Manet,[b] Sandra Monti,*[b] and Angelo Albini*[a]

Abstract: The irradiation in water of 1-ethyl-6,8-difluoro-7(3-methylpiperazino)3-quinolone-2-carboxylic acid (lomefloxacin), a bactericidal agent whose use is limited by its serious phototoxicity (and photomutagenicity in the mouse), leads to formation of the aryl cation in position eight that inserts into the 1-ethyl chain. Trapping of the cation was examined and it was found that chloride and bromide straightforwardly add in position eight, but with iodide and with pyrrole the 1-(2-iodoethyl) and the 1-[2-(2-pyrrolyl)ethyl] derivatives are formed. Flash photolysis reveals the triplet of lomefloxacin, a short-lived species ($\lambda_{max}=370$ nm, $\tau=40$ ns) that generates the triplet cation ($\lambda_{max}=480$ nm, $\tau\approx120$ ns). The last intermediate is quenched both by halides and by pyrrole. DFT and post-HF methods have shown that the triplet is the lowest state of the cation ($\Delta G_{ST}=13.3$ kcal mol^{-1}) and intersystem crossing (ISC) to the singlet has no role because a less endothermic process occurs, that is, intramolecular hydrogen abstraction from the *N*-ethyl chain (9.2 kcal mol^{-1}) that finally leads to cyclization. The halides form weak complexes with the triplet cation (k_q from 4.9×10^8 for Cl^- to 7.0×10^9 M^{-1} s^{-1} for I^-). With Cl^- and Br^- ISC occurs in the complex along with C_8–X bond formation. However, this latter process is slow with bulky iodide and with neutral pyrrole, and in these cases moderately endothermic electron transfer (ca. 7 kcal mol^{-1}) yielding the 8-quinolinyl radical occurs. Hydrogen exchange leads to a new radical on the 1-ethyl chain and to the observed products. These findings suggest that the mutagenic activity of the DNA-intercalated drug involves attack of the photogenerated cation to the heterocyclic bases.

Keywords: carbocations · cations · density functional calculations · fluoroquinolones · photochemistry

Introduction

In situ activation of drugs is an emerging research area and may open the way to new therapeutic applications, in particular for highly active and usually cytotoxic compounds, for which restricting the action to specific targets is of primary importance, as in the case of DNA-targeting antitumor drugs.[1a,b] Among the possible activation methods, photochemistry is distinguished by its ability to generate highly reactive intermediates under peculiarly mild conditions, provided that transmission of light to the desired target can be achieved and a suitable photoactivable moiety is present. Until now, photoinduced DNA alkylation has been obtained for a limited number of compounds, in most cases pertaining either to the group of psoralens[1c] or to that of quinone methides.[1d,e] Thus, it would be useful to devise further classes of molecules that can be photoactivated and damage selectively a cell component, in particular DNA. Inspiration for this search may be obtained by reviewing literature cases of the phototumorigenic effect of xenobiotics, in particular of drugs, because in this case the mechanism of action, and thus, the location in the cell, is known. Understanding how the noxious effect is caused may suggest a way for using

[a] Prof. M. Freccero, Prof. E. Fasani, Prof. M. Mella, Prof. A. Albini
Department of Organic Chemistry, University of Pavia
Via Taramelli 10, 27100 Pavia (Italy)
Fax: (+39) 0382-98323
E-mail: mauro.freccero@unipv.it
angelo.albini@unipv.it

[b] Dr. I. Manet, Dr. S. Monti
Istituto per la Sintesi Organica
e la Fotoreattività-ISOF, CNR Area della Ricerca
Via P. Gobetti 101, 40129 Bologna (Italy)
E-mail: monti@isof.cnr.it

Supporting information for this article is available on the WWW under http://www.chemeurj.org/ or from the author: Cartesian coordinates, energies, and thermal corrections to energy, enthalpy, and free energy of the stationary points.

that compound or some derivative for the selective attack on a tumor.

A case in point is that of the fluoroquinolone lomefloxacin (**1**), an inhibitor of bacterial gyrase[2,3] effective against a variety of infections, but presently less often used because of negative side effects, including significant phototoxicity. In fact, this drug is known to cause single-strand DNA cleavage and tumorigenesis in animals.[4,5] Indeed, the activity of **1** is so remarkable that this molecule has been proposed as a standard of photomutagenic action.[4] This distinguishes **1**, a 6,8-difluoro derivative, from most fluoroquinolones (bearing a single fluorine in position six) that do not exhibit such activity, although being somewhat phototoxic. The reason of this enhanced activity is unclear at present, although it has been ascertained that this is *not* due to a higher skin concentration after administration of the drug.[5a]

Interestingly, the mechanism underlying the photomutagenic effect of **1** seems to be peculiar. In fact, reactive oxygen species (ROS) have most often been suggested to be the active species in drug-photoinduced DNA damage [Eq. (1)]:

$$\text{drug} + h\nu \rightarrow {}^1\text{drug} \rightarrow {}^3\text{drug} + O_2 \rightarrow {}^1O_2 \text{ or } O_2^{\cdot -} \qquad (1)$$

However, in vitro experiments showed that oxygen activation yielding either $^1O_2$ or $O_2^{\cdot -}$ is modest in the case of **1**, but more efficient with other fluoroquinolones.[6a,b] Furthermore, photobiological studies showed that with this drug not only formation of 8-oxoguanine, the typical mark of oxidative damage,[6c,d] but also cyclobutane pyrimidine dimerization occurred[5b] and the latter phenomenon was correlated with UVA-induced tumorigenesis. The occurrence of pyrimidine dimerization suggests a different mechanism, that is, the initiating step is energy transfer from the drug in the triplet state[7] to the pyrimidine chromophore [Eq. (2)] and that this causes the damage:

$$\text{drug} + h\nu \rightarrow {}^1\text{drug} \rightarrow {}^3\text{drug} + \text{DNA base} \rightarrow {}^3\text{DNA base} \rightarrow \text{dimers} \qquad (2)$$

Evidence has been reported that this mechanism is involved in the phototoxic effect of monofluoroquinolones,[8] in agreement with the fact that such molecules exhibit a long-lived triplet ($\tau_T \approx 1$ μs), as indicated by flash photolysis studies in water.[9] However, once again lomefloxacin behaves differently, as only a weak absorption is observed in the place of the intense transient triplet signal of the monofluoro derivatives,[9] suggesting that triplet ^{3}**1** is short lived and the photophysical pathway of [Eq. (2)] is less likely. A final possibility is that irradiation causes a chemical reaction of the excited drug itself (or of a photoproduct of it) with DNA,[6e] possibly establishing a covalent bond [Eq. (3]:

$$\begin{aligned}&\text{drug} + h\nu \rightarrow {}^{1,3}\text{drug} + \text{DNA} \rightarrow \text{products}\\ &\text{or } {}^{1,3}\text{drug} \rightarrow \text{products}\\ &\text{products} + \text{DNA} \rightarrow \text{products}\end{aligned} \qquad (3)$$

On the basis of the foregoing, it appears that searching for a mechanism of the photomutagenic and genotoxic effect by lomefloxacin has a more general interest than assessing a limitation in the therapeutic use of this molecule. An unusual mechanism may be involved, based on a photoreaction of the drug with a biomolecule [Eq. (3)], which may be the model for a new class of photoactivated drugs. However, it is difficult to guess from literature reports which bimolecular reaction may be involved, because irradiation of **1** in water[10a] (as well as in plasma)[10b] causes an efficient ($\Phi = 0.55$) unimolecular reaction to give pyrroloquinolone **3**. Evidence that this process involves heterolysis of the C_8–F bond to form carbocation $\mathbf{2}^+$ that inserts into the β position of the *N*-ethyl group (see Scheme 1) was presented.[10a] Furthermore, a transient attributed to this cation has been detected by flash photolysis (see below).[11] Thus, a highly reactive intermediate, such as aryl cation $\mathbf{2}^+$,[12,13] is generated by photolysis, but is consumed *intramolecularly*, with no interference even by solvent water (no 8-hydroxyquinolone **3′** is formed).[14]

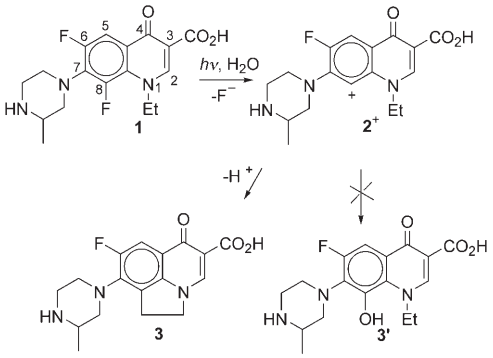

Scheme 1. Photoreaction of **1** in water.

Results

Photochemical studies: In view of the above, an in-depth study of the photochemistry of lomefloxacin appeared worthwhile. As shown in the following, intriguing results were obtained and elaborated computational work was required for the rationalization. In previous work, we had identified an intermolecular reaction via cation $\mathbf{2}^+$, that is, Cl/F exchange at position eight leading to compound **4a** by irradiation of **1** in the presence of NaCl (Scheme 2).[15] The efficiency of chloride trapping was determined by measuring the ratio of the cyclization yields in the presence vs in the absence of Cl^-. According to Scheme 2, the ratio of the cyclized product **3** in the presence vs in the absence of the anion was expected to depend linearly on the Cl^- concentration, $[\mathbf{3}]/[\mathbf{3}]^0 = 1 + (k_{Cl}/k_i)\,[Cl^-]$. This was indeed observed with Cl^- (under constant ionic strength, obtained by adding a suitable amount of $NaClO_4$, see Experimental Section) and the rate-constants ratio for chloride addition versus intramolecular insertion could be calculated, $k_{Cl}/k_i = 60\ \text{M}^{-1}$.

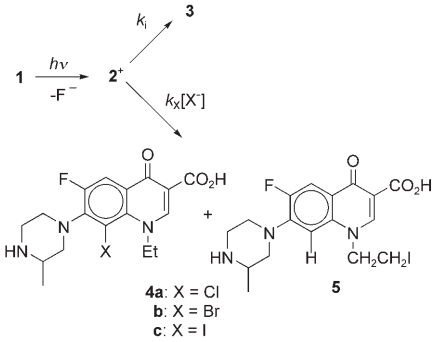

Scheme 2. Photoreaction of **1** with halides.

We now further tested the irradiation in the presence of halides, and found that with bromide the analogous bromoquinolone **4b** was formed (70% vs 3% **3** with 0.05 M NaBr at 35% conversion of **1**; further irradiation caused a significant reductive debromination of **4b**, a secondary photoreaction as proven by separate irradiation of pure **4b**). Trapping was more efficient than with chloride ($k_{Br}/k_i = 520\,M^{-1}$). As for fluoride, an effect was obtained only when a large amount was added and involved a slowing of the photoconversion of **1** to **3**, reasonably because fluoride intercepted the cation to give back the starting compound. By treating the data as above, the rate ratio was measured as $k_F/k_i = 5\,M^{-1}$.

When iodide was considered, a faster reaction was observed ($k_I/k_i = 915\,M^{-1}$), but the striking fact was that the product *structure* was different. The main product did result from overall F/I exchange, but position eight was reduced and the iodine atom was located on the *N*-ethyl chain in the β position (structure **5**), as indicated by spectroscopic analysis (see Experimental Section). The expected 8-iodo derivative (**4c**) was only a minor product (62% **5**, 7% **4c**, traces of **3** with 0.05 M NaI at 25% conversion).

Recalling that phenyl cations are known to react with π nucleophiles,[13] fluoroquinolone **1** was irradiated also in the presence of pyrrole. Indeed, a new product was formed that incorporated the heterocycle, characterized by reductive defluorination in position eight and insertion of pyrrole into the ethyl side chain (product **6**, Scheme 3).

Thus, a diagnostic trapping of cation $\mathbf{2^+}$ occurred in the presence of both halide anions and of a neutral π nucleophile such as pyrrole (not of a neutral n nucleophile such as water, though). However, two

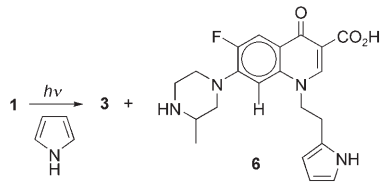

Scheme 3. Photoreaction of **1** with pyrrole.

different reaction paths were involved, with attack either at C_8 or at the side chain β position. We further checked that quenching of the fluorescence of **1** was modest ($K_{SV} = 3\,M^{-1}$ for pyrrole).

Detection of transients: Laser flash photolysis experiments at $\lambda_{exc} = 355$ nm have been carried out both by ourselves[9] and, more recently, by Cuquerella et al.[11] We reported a weak shortlived absorption (λ_{max} ca. 500 nm), that the latter authors evidenced to be quenched by chloride and bromide ($k_{Cl} = 4.1 \times 10^8$, $k_{Br} = 3.6 \times 10^9\,M^{-1}s^{-1}$). However, an accurate reexamination of the evolution of the spectra now revealed that there were actually *two* short-lived transients. The difference spectrum taken at 25 ns from pulse end was characterized by two main bands peaking at 370 and 480 nm (see Figure 1). Time evolution occurred by biexponential kinetics, the absorbance profiles clearly exhibiting a growing phase followed by a decay at 480 nm and a monotonic decrease toward a constant value at 370 nm. Neither of the two bands was appreciably quenched by O_2 or N_2O.

A kinetic model with three species involved in two consecutive reactions with rate constants k_1 and k_2 proved to suit perfectly the whole spectral range. The separated spectra of these species (difference spectra with respect to the ground state of **1**) were reconstructed by means of the

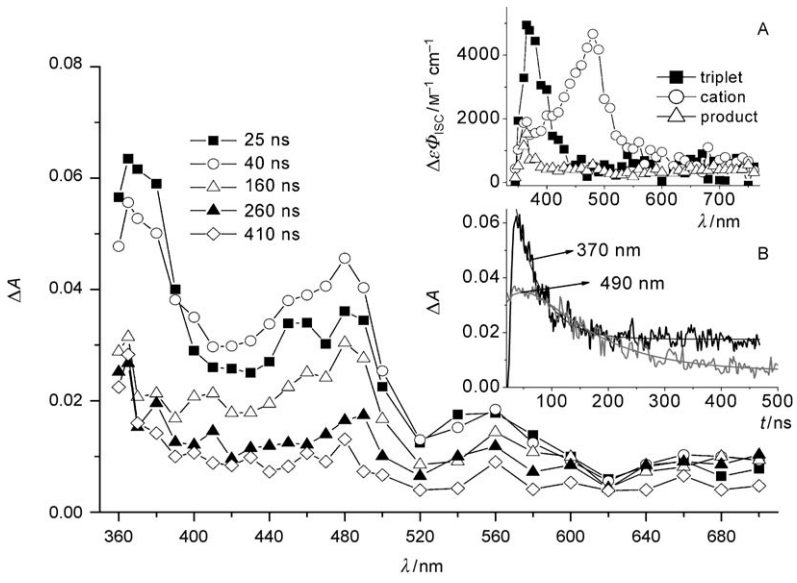

Figure 1. Transient absorption spectra upon excitation at 355 nm of an N_2O saturated 1.4×10^{-3} M solution of **1** in 1×10^{-3} M $NaHCO_3$ buffer of pH 6.9 at 25 °C at various delays from pulse end. Insets: A) reconstructed absolute spectra and B) kinetics at 370 nm (black) and 490 nm (grey).

SPECFIT/32 program, using the time constants $k_1=(2.5\pm0.3)\times10^7\,s^{-1}$ and $k_2=(8.3\pm0.2)\times10^6\,s^{-1}$ and are shown in inset A of Figure 1.

The above-mentioned quenching by chloride and bromide was confirmed, but this involved *only* the 480 nm band. The same applied to iodide, as can be appreciated in Figure 2. Particularly instructive were experiments at a low concentration of the quencher. With iodide at 5×10^{-4} M it could be clearly distinguished that the 370–380 nm band was not quenched, whereas the 480–490 nm was (see insets A and B). Furthermore, the 490 nm band in turn evolved toward a much longer-lived absorption evidenced at 345 nm (compare the formation profile shown in inset C with the decay in inset A).

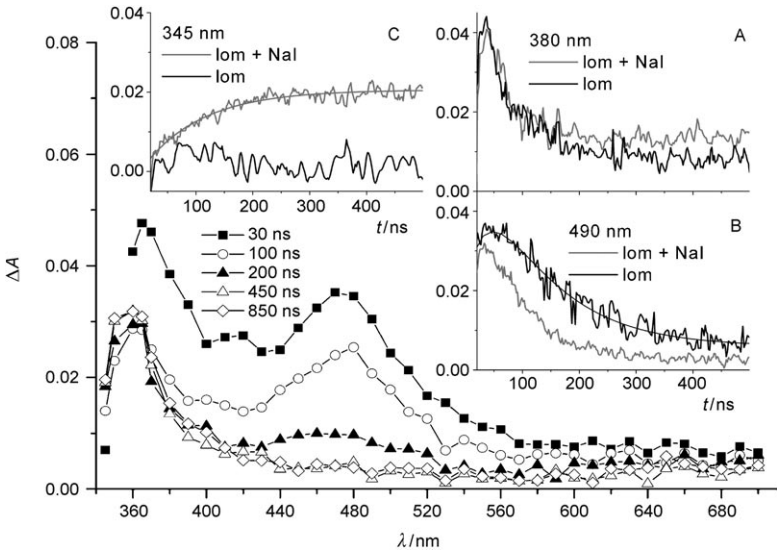

Figure 2. Transient absorption spectra upon excitation at 355 nm of an N_2O saturated 1.4×10^{-3} M solution of **1** in the presence of 0.5×10^{-3} M NaI in 1×10^{-3} M $NaHCO_3$ buffer of pH 6.9 at 25 °C at various delays from pulse end. Insets: kinetics at A) 380 nm, B) 490 nm, and C) 345 nm in the absence (black) and presence of NaI (grey [NaI] = 1×10^{-3} M for 490 nm).

Figure 3 shows the results obtained in the presence of pyrrole. With 5×10^{-2} M of quencher, the formation of an absorption in the region 450–520 nm was barely observable, whereas the 365 nm absorption disappeared with practically unchanged kinetics (see inset). At 5×10^{-3} M, pyrrole had little effect on the observed transients.

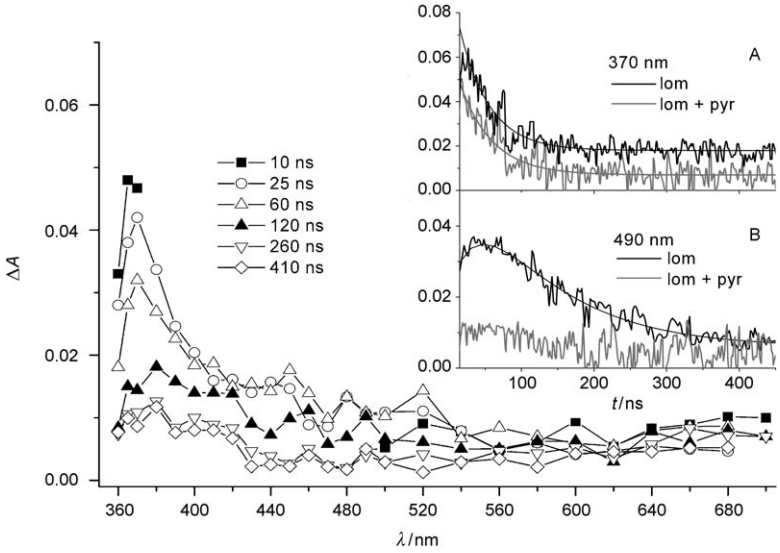

Figure 3. Transient absorption spectra upon excitation at 355 nm of an N_2O saturated 1.4×10^{-3} M solution of **1** in the presence of 0.05 M pyrrole in 1×10^{-3} M $NaHCO_3$ buffer of pH 6.9 at 25 °C at various delays from pulse end. Insets: kinetics at 370 nm and 490 nm in the absence (black) and presence (grey) of 0.05 M pyrrole.

The above experiment show that the first-formed transient, absorbing more strongly in the near UV region ($\lambda_{max}=365$ nm, $\tau\cong40$ ns), was *not* quenched by either halides or pyrrole and was the precursor of the further transient in the visible region ($\lambda_{max}=480$ nm and lifetime ca. 120 ns), the one that was quenched. Besides confirming the quenching constants already reported for Cl^- and Br^-, we further measured the constant for iodide ($k_I=7.0\times10^9\,M^{-1}s^{-1}$) and estimated a lower limit for that for pyrrole ($k_{py}>2\times10^9\,M^{-1}s^{-1}$). [The rate constant for the trapping of the second intermediate by pyrrole was estimated as $k_{py}>2\times10^9\,M^{-1}s^{-1}$, considering that this intermediate did not appreciably accumulate at [Py] of 5×10^{-2} M and thus, the decay rate in the presence of a quencher (k'_2) must be markedly larger than its rate of formation ($k_1=2.5\times10^7\,s^{-1}$). Thus, for a k'_2/k_1 ratio $>\approx4$, it resulted that k_{py} [py] $>\approx1\times10^8\,s^{-1}$.]

Computational Studies

Geometry and energy of the cation spin states: The formation of products **5** and **6** and the change in product distribution in going from bromide to iodide were quite puzzling. This fostered computational work, aimed to model the prop-

erties and the reactivity of the suggested intermediate cation $\mathbf{2}^+$ and to test whether the experimentally observed two modes of trapping were reproduced. This was done in gas and condensed phases by using DFT and post-HF methods.

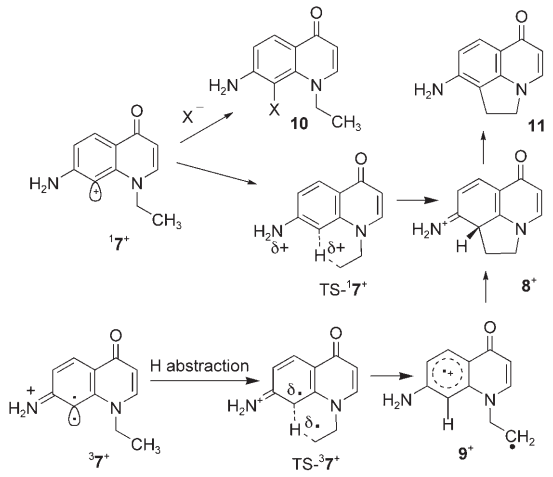

Scheme 4. Calculated intramolecular paths from quinolinyl ion $\mathbf{7}^+$.

A somewhat simplified model structure that incorporated the essential features of $\mathbf{2}^+$ was used, namely, 7-amino-1-ethyl-4-oxo-1,4-dihydro-quinolin-8-yl cation ($\mathbf{7}^+$, see Scheme 4).

DFT and MP2 calculations were performed at U(R)B3LYP/6-31+G(d,p) and MP2/6-31+G(d,p) levels of theory. Solvation effects on geometries and energies were computed by means of the polarizable continuum model (PCM) using both UA0 and UAHF radii (see Supporting Information for details). Of the two spin states of the cation, both DFT and post-HF methods predicted in good agreement a planar geometry for triplet $^3\mathbf{7}^+$ and a puckered aromatic ring for singlet $^1\mathbf{7}^+$ (Figure 4). Both methods predicted the triplet to be more stable than the singlet, but the MP2 method seemed to overestimate the stability of the open-shell species. At the U(R)B3LYP/6-31+G(d,p) level of theory $\Delta E_{T-S} = 13.6$ kcal mol^{-1} was predicted in the gas phase, with a minimal solvation effect (13.3 kcal mol^{-1} in water, see Table 1).

Monomolecular reactivity of singlet and triplet aminoquinolinyl cations: Next, the potential energy surface (PES) of the unimolecular reactions involving the singlet and triplet aminoaryl cations $^1\mathbf{7}^+$ and $^3\mathbf{7}^+$ was explored to locate a viable path for the observed intramolecular attack on the *N*-ethyl chain. The stationary points (minima and transitions states, TSs) were searched for both in the gas phase and in aqueous solution (by using the PCM solvation model).

A path involving intramolecular insertion into the carbon–hydrogen bond was characterized for the singlet cation (see Scheme 4 and Table 1). This was an almost barrierless process in water, with an early transition state **TS**-$^1\mathbf{7}^+$ ($\Delta G^{\neq}_{H_2O} = 0.6$–$1.1$ kcal mol^{-1}, depending on solvent-cavity definition, see Figure 5).[16] From this TS the system evolved along the reaction coordinate toward a much more stable ($\Delta G^{\neq}_{H_2O} = -78.9$ kcal mol^{-1}) intermediate, a benzenium (Wheland) cation ($\mathbf{8}^+$), and hence to pyrroloquinoline **11**.

On the other hand, hydrogen abstraction was the viable path from the most stable state of the cation, triplet $^3\mathbf{7}^+$, and led to a triplet diradical cation, $\mathbf{9}^+$, by passing through **TS**-$^3\mathbf{7}^+$. This required an activation

Table 1. Electronic energies (E, in Hartree), relative electronic energies (ΔE_{gas}, in kcal mol^{-1}), thermal contribution to free energy (δG), free energy in the gas phase relative to $^1\mathbf{7}^+$ (ΔG_{gas}), free energy in aqueous solution (G_{sol}), free energy in aqueous solution relative to $^1\mathbf{7}^+$ (ΔG_{H_2O}), reaction free energy ($\Delta G^{\neq}_{H_2O}$) for quinolinyl cations $\mathbf{7}^+$ and some of their derivatives.

Stationary points	$-E$	ΔE_{gas}	δG	ΔG_{gas}	$-G_{sol}$	ΔG_{H_2O}	$\Delta G^{\neq}_{H_2O}$
$^1\mathbf{7}^+$	610.2013657[a]	0.0	100.4	0.0	610.282163[a,c]	0.0	–
	(606.386342015)[b]	(0.0)		(0.0)	610.290864[a,d]	0.0	
					(606.476167)[b,c]		
					(606.484550)[b,d]		
$^3\mathbf{7}^+$	610.2233267[a]	−13.8	100.2	−13.6	610.303710[a,c]	−13.3[a,c]	–
	(606.450723523)[b]	(−40.4)			610.312659[a,d]	−13.5[a,d]	
					(606.550972)[b,c]	−46.9[b,c]	
					(606.559549)[b,d]	−47.1[b,d]	
TS-$^1\mathbf{7}^+$	–[f]		99.8[g]		610.280461[a,c,e]	1.1	1.1
					610.289827[a,d,e]	0.6	0.6
TS-$^3\mathbf{7}^+$	610.2063026[a]	−3.1	98.3	–5.2	610.290895[a,c,e]	−8.8[a,c]	9.2
					610.294337[a,d,e]	−4.3[a,d]	
$\mathbf{8}^+$	610.3227159[a]	−76.1	106.1	−70.4	610.417001[a,c]	−78.9	−78.9
$\mathbf{9}^+$	610.2404845[a]	−24.5	99.6	−25.5	610.323023[a,c]	−26.4	−13.1
					610.330062[a,d]	−25.4	−11.9

[a] U(R)B3LYP/6-31G+(d,p). [b] U(R)MP2/6-31G+(d,p). [c] UA0 radii. [d] UAHF radii. [e] Adding a sphere to the hydrogen that is going to be transferred. [f] **TS**-$^1\mathbf{7}^+$ not located at the RB3LYP/6-31G+(d,p) level of theory in the gas phase. [g] In water solution at the RB3LYP/6-31G+(d,p) level.

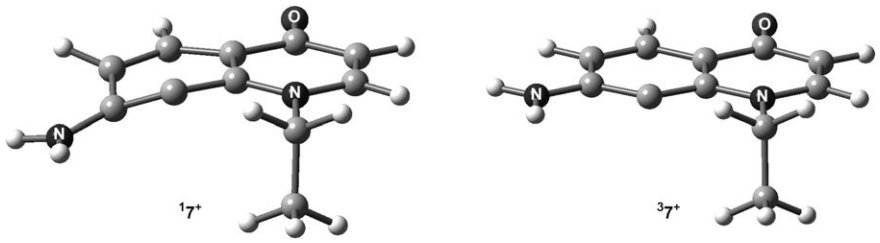

Figure 4. Geometries of singlet and triplet aminoaryl cations $^{1,3}\mathbf{7}^+$ in gas phase at the B3LYP/6-31+G(d,p) level.

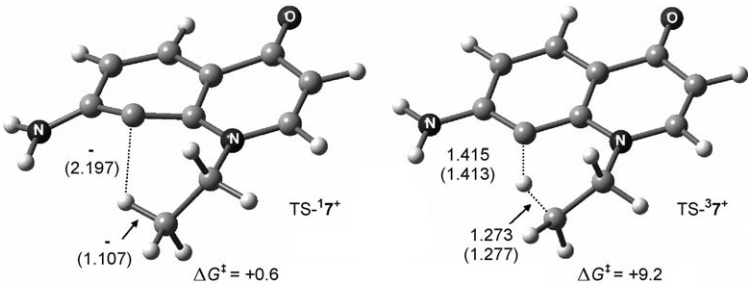

Figure 5. Calculated transition states **TS**-^{1}**7**$^+$ and **TS**-^{3}**7**$^+$. Reaction activation free energies (in kcal mol^{-1}) and distances (in Å) are shown for both the gas phase and aqueous solution (in parentheses), at the B3LYP/6-31+G(d,p) level.

free energy of 9.2 kcal mol^{-1} in water. In turn, cation **9**$^+$ could undergo intersystem crossing and cyclize to the above isomer **8**$^+$. As seen above, cyclization to **11** (Scheme 4) was indeed the experimentally observed process in the irradiation of lomefloxacin in water and calculations revealed that both the singlet and the triplet ions could be the intermediates in it, through a non-activated and activated path, respectively (see below).

Bimolecular reactivity of singlet and triplet aminoquinolinyl cations: As intuitively expected, singlet cation ^{1}**7**$^+$ collapsed to the corresponding eight-halo derivative (see structure **10**, Scheme 4) when in the vicinity of a halide anion. In contrast, computation evidenced that approaching of a chloride, bromide, or iodide anion to triplet cation ^{3}**7**$^+$ did not lead to bond formation, but to electrostatic pairing with the anion close to the 7-amino group, which bore most of the positive charge (see Figure 6).

The complexes were marginally stabilized in water, the net stabilization resulting from the opposite contributions of ion pairing and of loss of the solvation of the halide anion, respectively decreasing and increasing with the atomic weight of the halide (see Table 2). This was an important point because triplet cation ^{3}**7**$^+$ would have to undergo intersystem crossing (ISC) to ^{1}**7**$^+$ before coupling with the halide to give products **10**, and the previous formation of a complex might provide this opportunity, favored by the heavy-atom effect in the decreasing series $I^- \rightarrow Br^- \rightarrow Cl^-$ (see Discussion).

Table 2. Reaction free energy ($\Delta G_{complex}$) for the complexation of triplet cation **7**$^+$ by Cl^-, Br^-, and I^- in the gas phase ($\Delta G_{complex\text{-}gas}$) and in aqueous solution ($\Delta G_{complex\text{-}aq}$).

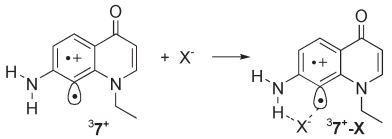

Complex ^{3}**7**$^+$-X$^-$	$\Delta G_{complex\text{-}gas}$	$\Delta G_{complex\text{-}aq}$	ΔG_{sol} X$^-$
^{3}**7**$^+$-Cl$^-$	−112.1[a]	−0.2[a]	−74.6
^{3}**7**$^+$-Br$^-$	−119.3[b]	−11.1[b]	−68.6
	−106.9[c]	+0.6[c]	
^{3}**7**$^+$-I$^-$	−102.7[c]	−2.3[c]	−60.7

[a] At the B3LYP/6-31+G(d,p) level of theory. [b] At B3LYP/6-31+G(d,p) with LAN2DZ basis set for Br^-. [c] At B3LYP/6-31+G(d,p) with CEP-31G basis set for Br^- and I^-.

As mentioned above, the experiments showed that products of type **10** were formed with Cl^- and Br^-, but of type **12** with iodide (see Scheme 5). This changed path must be rationalized. Because it involved the side chain, just as cyclization to **11**, a possibility was that **12** arose from the same intermediate as cyclization, namely, from cation **8**$^+$. It may be thought that this reacted in two ways. Thus, in the conversion of **8**$^+$ to **11** water acted as a base. Should it act as a nucleophile, ring opening to give a product of structure **12** would indeed result. The viability of these mechanisms was tested computationally, by locating the transition state from **8**$^+$ to **11** in water [**TS**-**8**$^+$-**11**(H_2O)] and toward **12** with either water [**TS**-**8**$^+$-**12**(H_2O)] or I^- as the nucleophile [**TS**-**8**$^+$-**12**(I^-)]. At the B3LYP level of theory, using both 6-31G(d) and 6-31+(d,p) basis sets, the ring-

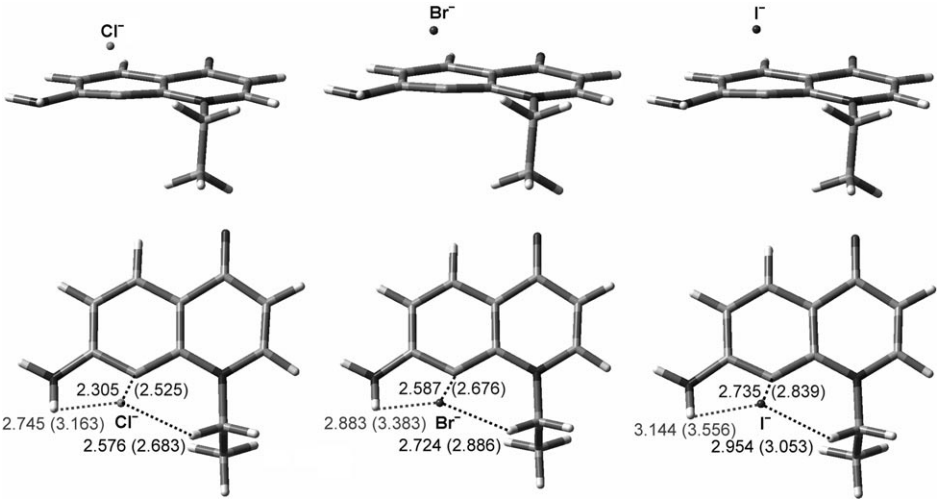

Figure 6. Side and upper views of the complexes ^{3}**7**–X at the B3LYP/6-31+G(d,p) level with CEP-31G basis set for Br^- and I^-, in the gas phase and in aqueous solution (in parenthesis). LAN2DZ basis set for Br^- gives very similar geometries.

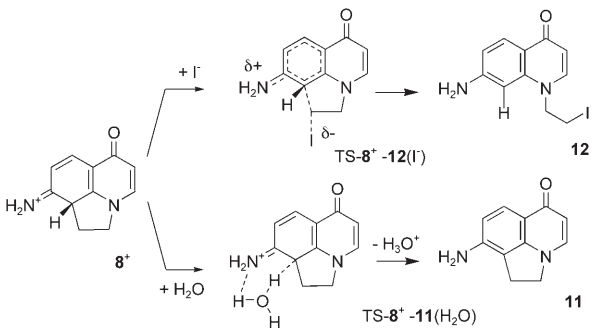

Scheme 5. Possible reactions of cation $\mathbf{8}^+$ with bases/nucleophiles.

opening processes induced by water and iodide anion were largely endothermic in aqueous solution, with an activation free energy greater than 37 kcal mol^{-1}. In contrast, the deprotonation of the Wheland cation $\mathbf{8}^+$ to give **11** was a barrierless process (Table 3).

Table 3. Activation free energy in the gas phase ($\Delta G^{\neq}_{gas}$ in kcal mol^{-1}) and in aqueous solution ($\Delta G^{\neq}_{H_2O}$), relative to the complexes $\mathbf{8}^+$–H_2O and $\mathbf{8}^+$–I^-, for the transition states involved in the deprotonation and ring-opening reactions of benzenium cation $\mathbf{8}^+$.

Stationary points	$\Delta G^{\neq}_{gas}$	$\Delta G^{\neq}_{H_2O}$
TS-8$^+$-11(H_2O)	32.8[a] (32.2)[b]	_[c]
TS-8$^+$-12(H_2O)	61.9[a] (61.8)[b]	48.2[d]
TS-8$^+$-12(I^-)	34.0[e]	37.5[f]

[a] B3LYP/6-31G(d) [b] B3LYP/6-31+G(d,p). [c] No TS was located in water, deprotonation occurred with no barrier in the presence of an ancillary water molecule. [d] PCM-B3LYP/6-31+G(d,p). [e] B3LYP/6-31G(d) and CEP basis set on I^-. [f] PCM-B3LYP/6-31G(d) and CEP basis set on iodide anion.

Thus, this mechanism did not explain the reaction with iodide (and the analogous process with pyrrole), which must involve interaction of the nucleophile directly with ion $\mathbf{7}^+$, and yet differ from simple coupling that would give product **11**. An alternative we considered was that an electron-transfer process was occurring, rather than an electrophile–nucleophile combination. The thermochemistry of the monoelectronic reduction of both spin states of the cation ($^{1,3}\mathbf{7}^+$) to quinolinyl radical $\mathbf{7}^\cdot$ by iodide anion and by pyrrole was evaluated in aqueous solution. The free-energy change for the vertical oxidation of pyrrole to its radical cation and the vertical reduction of ions $\mathbf{7}^+$ were computed at B3LYP/6-31G+(d,p) level of theory, and that for the reduction of iodide radical to iodide anion at B3LYP/CEP-31G and B3LYP/Lan2DZ by using the PCM solvation model. It was gratifying to find that the computational results were close to the experimental data where available. Thus, the calculated free-energy change for the I$^\cdot$/I$^-$ process and that obtained from the measured redox potential through a thermochemical cycle [E(I$^\cdot$+e$\rightarrow$I$^-$) +1.33 V vs normal hydrogen electrode (NHE),[17a] calculated by taking $G_{gas,H^+} = -6.28$ kcal mol^{-1}, $G_{solv,H^+} = -262.23$ kcal mol^{-1},[17b] and $\Delta H_f(H_2) =$ 104.1 kcal mol^{-1}] were very similar, and the same held for pyrrole (experimental E_{ox} 1.31 V).[18]

The results are gathered in Table 4 and suggest that the monoelectronic reduction of both cations $^{1,3}\mathbf{7}^+$ by iodide anion was slightly endoergonic (5 to 7 kcal mol^{-1}, see footnotes of Table 4) and virtually identical data were obtained for pyrrole.

Table 4. Computed (vertical) reduction potentials of triplet ($^3\mathbf{7}^+$) and singlet ($^1\mathbf{7}^+$) quinolonyl cations, of cation $\mathbf{9}^+$, iodine atom, and pyrrole radical cation in aqueous solution, compared to experimental values (for iodine and pyrrole).

Redox reaction	E [V] (vs NHE)
I$^\cdot$→I$^-$	+1.33,[a] 1.30[b]
$^1\mathbf{7}^+$→$\mathbf{7}^\cdot$(v)	+1.12[c]
$^3\mathbf{7}^+$→$\mathbf{7}^\cdot$(v)	+1.02[c]
pyrrole$^{\cdot+}$(v)+e→pyrrole	+1.31,[a] 1.35[c]
$\mathbf{9}^+$→$\mathbf{13}^\cdot$	+1.12[c]

[a] Experimental value. [b] Computed at B3LYP/LAN2DZ with solvation effects evaluated by the PCM solvation model using UA0 radii, and taking into account $G_{gas,H^+} = -6.28$ kcal mol^{-1}, $G_{solv,H^+} = -262.23$ kcal mol^{-1}, $\Delta H_f(H_2) = 104.1$ kcal mol^{-1}. [c] Calculated from the computed activation free energy in water [at PCM-U(R)B3LYP/6-31G+(d,p) using LAN2DZ for I$^-$] for the reactions: $^1\mathbf{7}^+ + I^- \rightarrow \mathbf{7}^\cdot(v) + I^\cdot + 4.9$ kcal mol^{-1}; $^3\mathbf{7}^+ + I^- \rightarrow \mathbf{7}^\cdot(v) + I^\cdot + 7.2$ kcal mol^{-1}; pyrrole$^{\cdot+}$(v)+I$^-$→pyrrole+I$^\cdot$−0.4 kcal mol^{-1}; $\mathbf{9}^+ + I^- \rightarrow \mathbf{13}^\cdot + I^\cdot + 4.9$ kcal mol^{-1}; taking into consideration the experimental redox potential for the couple I$^\cdot$/I$^-$ (1.33 V, vs NHE) by $\Delta G = -nF[\Delta E(^1\mathbf{7}^+/\mathbf{7}^\cdot) - \Delta E(I^\cdot/I^-)]$.

Electron-transfer path: It appeared unlikely that electron transfer was important for singlet $^1\mathbf{7}^+$, for which a barrierless intramolecular process was available to give $\mathbf{8}^+$ (although coupling with a paired anion to give **10** may compete). However, in the case of the triplet cation, reduction to radical $\mathbf{7}^\cdot$ by iodide (or pyrrole) confronted a lower barrier than hydrogen abstraction (7.2 vs 9.2 kcal mol^{-1}). The ensuing chemistry of the radical was explored and this was found to convert, after thermal relaxation, to the alkyl radical $\mathbf{13}^\cdot$ (Scheme 6) by intramolecular hydrogen abstraction from the ethyl side chain. The first-order saddle point **TS-7**$^\cdot$ connecting $\mathbf{7}^\cdot$ to $\mathbf{13}^\cdot$ lay only 3.8 kcal mol^{-1} above the reactant in water, therefore, it did not represent the rate-determining step of this reaction (Figure 7).

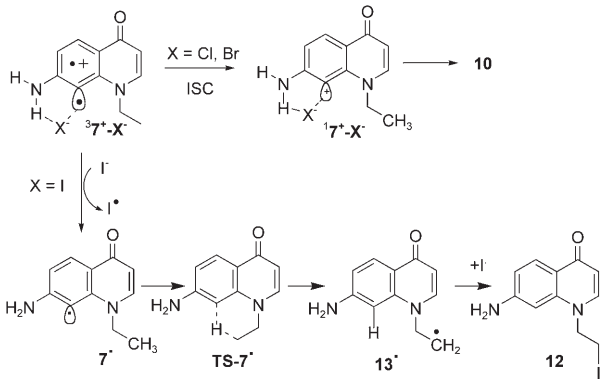

Scheme 6. Electron-transfer path from cation $^3\mathbf{7}^+$.

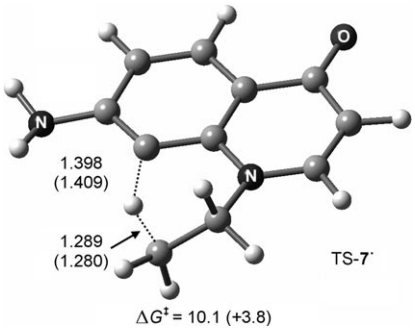

Figure 7. Structure of transition state **TS-7˙**. Reaction activation free energy (in kcal mol^{-1}) and distances (in Å) are shown for both the gas phase and aqueous solution (in parentheses), at the B3LYP/6-31+G(d,p) level.

In turn, this alkyl radical could react with I^- or co-formed iodine atom (or, respectively, with pyrrole or its radical cation) to generate the final products **12** (Scheme 6). Further calculations showed that distonic diradical cation $\mathbf{9}^+$ was also reduced to radical **13˙** at an accessible potential and electron transfer from iodide and pyrrole was likewise slightly endothermic (4.3 and 6.6 kcal mol^{-1}, respectively), thereby offering a further path to 12 (Table 5).

Table 5. Electronic energies (E, in Hartree), relative electronic energies (ΔE_{gas}, in kcal mol^{-1}), thermal contribution to free energy (δG), relative (to **7˙**) free energy in the gas phase (ΔG_{gas}), free energy in aqueous solution (G_{H_2O}), relative (to **7˙**), free energy in aqueous solution (ΔG_{H_2O}) for radicalic intermediates and transition states.

Stationary points	$-E$	ΔE_{gas}	δG	ΔG_{gas}	$-G_{H_2O}$	ΔG_{H_2O}
7˙	610.4958393[a]	0.0	101.2	0.0	610.508769[a,b]	0.0
TS-7˙	610.4763145[a]	12.3	99.0	10.1	610.499151[a,b]	3.8
13˙	610.51024[a]	−9.0	99.9	−10.3	610.527240[a,b]	−12.9

[a] U(R)B3LYP/6-31G+(d,p). [b] UA0 radii.

Discussion

Previous evidence indicated that the photochemistry of lomefloxacin (**1**) in water involved release of fluoride selectively from position eight and the process was unimolecular with a reaction quantum yield Φ_r of 0.55, much higher than that exhibited by 6-monofluoroquinolones, not undergoing unimolecular cleavage (e.g., 0.06 for norfloxacin). Because the fluorescence quantum yields and lifetimes of 6,8-difluoroquinolones such as **1** and 6-monofluoroquinolone derivatives are similar (e.g., $\Phi_F = 0.08$ for **1** and 0.11 for norfloxacin, with $\tau_F = 1$ and 1.5 ns, respectively), photofragmentation should not occur from the singlet excited state.

On the other hand, the large increase in *reaction* quantum yield was accompanied by a dramatic change in the T–T absorption. Monofluoroquinolones exhibit an intense and relatively long-lived triplet absorption ($\tau = 1$ μs) with λ_{max} in the range 500–620 nm.[8] In the case of **1**, careful examination of the time-resolved spectra evidences a short-lived (ca. 40 ns) transient absorbing at around 370 nm (Figure 1), unaffected by the additives tested, that fits well with the expectation of a triplet undergoing a fast monomolecular fragmentation. In fact, comparing the lifetime of this state (^{3}**1**, 40 ns) with that of the monofluoroquinolones (ca. 1 μs), suggests that fragmentation occurs with an efficiency of around 95%, well in accord with the high quantum yield of the photoreaction; the short lifetime explains the lack of O_2 quenching. The reconstructed spectra show that ^{3}**1** has no absorption in the visible region and is the precursor of a further transient with $\lambda_{max} = 480$ nm (Figure 1). The latter is again unaffected by O_2, but *is* quenched by halides (rate increases to diffusion-controlled with iodide) and by pyrrole. If this were the singlet cation, one would expect that coupling with any anion, with no spin barrier, would occur at the same rate. The observed difference supports that the latter transient is triplet cation $^3\mathbf{2}^+$ (see below), which is the expected state from the cleavage of triplet ^{3}**1**.

The computational study on the simplified model $\mathbf{7}^+$ showed that the two spin states of the cation are quite different in structure and chemistry. As far as the structure is concerned, the difference mirrored that found with 4-aminophenyl cation, with the planar triplet lowest in energy and the singlet (ca. 13 kcal mol^{-1} above it) characterized by a puckering out of plane of C_8. Again, as with phenyl cations, the singlet is a localized cation with an empty σ orbital at C_8, whereas the triplet has one electron in the σ orbital and one unpaired electron in the aromatic π system. This endows the aromatic moiety with radical-cation character, with strong donation from the amino group (see the simplified structures in Scheme 4).

Examination of the potential energy surface (PES) for the reactions of the two states of the cation evidenced a well-differentiated chemistry. In the case of singlet $^1\mathbf{7}^+$, intramolecular insertion in the β C–H bond is facile, with an early (and barely observable) transition state. The detailed mapping of this process highlighted a close resemblance with insertion reactions via singlet carbenes,[19] with simultaneous rotation of the ethyl group and bond formation. The triplet quinolinyl cation, on the other hand, has no non-activated path available. The most favorable reaction channel, hydrogen abstraction to give distonic diradical cation $\mathbf{9}^+$, confronts a 9.2 kcal mol^{-1} barrier. With two unpaired electrons in two orthogonal orbitals, $^3\mathbf{7}^+$ resembles a triplet carbene or a radical at C_8. Indeed, comparison of the structures of cation $^3\mathbf{7}^+$ and radical **7˙**, as well as the almost identical transition states for hydrogen abstraction, **TS**-$^3\mathbf{7}^+$ and **TS-7˙** (see Figures 5 and 7) demonstrates that the triplet cation has a well-defined sp^2 radical character at C_8.

To summarize, intermediate $^3\mathbf{7}^+$ is formed first, but has only activated paths available, leading either to diradicalic $\mathbf{9}^+$ or to $^1\mathbf{7}^+$ through ISC, both paths finally reaching cyclized **11**. The latter path, however, confronts a markedly higher (by more than 5 kcal mol^{-1}) barrier and thus, it ap-

pears unlikely that the singlet is formed even as a secondary intermediate and, if it were formed, the steeply descending path leading to $\mathbf{8}^+$ and entropic factors would make trapping difficult.

As for intermolecular processes, these do not involve the excited states, as the quenching of both the fluorescence and the T–T absorption is unimportant under the conditions used. Indeed, experiments showed that both types of products, the 8-substituted quinolones **10** and products **12** bearing the substituent at the β-ethyl position, arise from a *single* intermediate, the transient detected at 480 nm in flash photolysis and identified as the triplet cation, as supported by the correspondence of the rate-constants ratio from flash photolysis ($Cl^-/Br^-/I^-$ 1:11.2:14.0) with those from steady-state experiments ($F^-/Cl^-/Br^-/I^- = 0.08:1:8.7:15.3$). No further common intermediate is involved, as a thorough search for a nucleophile-driven ring opening in cation $\mathbf{8}^+$ gave no result, proving that this path leads only to cyclized **11**.

The different quenching rates of the 480 nm transient supports, as mentioned, the triplet multiplicity. Furthermore, the observed fast increase as the atomic weight of the halide quencher increases confirms that heavy-atom-induced ISC has a role. Thus, it seems reasonable to conclude that ISC from $^3\mathbf{7}^+$ to $^1\mathbf{7}^+$ is insignificant in neat water because of the high endothermicity. In the weakly stabilized $^3\mathbf{7}^+$–X^- complex (see Figure 6) the barrier is much lower, as ISC in the cation occurs simultaneously with the highly exothermic coupling with the anion to give the 8-halogeno derivatives **10** (Scheme 6). However, when passing from Cl^- and Br^- to bulky I^- bond formation at position eight, flanked by branched substituents at both sides, is expected to slow down. The other path individuated by computation is electron transfer that is favored with a good oxidant, such as iodide, which is in fact active at very low concentrations (Figure 2). Likewise, a neutral nucleophile such as pyrrole is not sufficiently reactive for attacking the hindered electrophilic site in cation $\mathbf{7}^+$, but being a good donor it reacts through electron transfer to give a product of type **12**, just like iodide. Electron transfer is an activated process, but with a smaller barrier than hydrogen abstraction, and occurs according to the sequence $^3\mathbf{7}^+ \rightarrow \mathbf{7}^\bullet \rightarrow \mathbf{13}^\bullet$ (with activation energy of the first, and rate-determining, step, of 6–7 kcal mol^{-1}), or, less likely, after hydrogen abstraction ($^3\mathbf{7}^+ \rightarrow \mathbf{9}^+ \rightarrow \mathbf{13}^\bullet$, activation energy of the first step, 9.2 kcal mol^{-1}). Finally, the change in mechanism is characterized by the appearance of a new transient that arises from $^3\mathbf{7}^+$ (see inset C in Figure 2); this may correspond to radical $\mathbf{7}^\bullet$.

Thus, the two different intermolecular reactions arise from the triplet cation $^3\mathbf{7}^+$, either through ISC in the complex and ionic coupling or through electron transfer, respectively, the choice between the two paths being determined by the bulk and the oxidation potential of the quencher.

The rationalization of the photochemistry of fluoroquinolone **1** presented above suggests a mechanism for the observed mutagenic effect that fits with the experimental results. Photolysis of lomefloxacin in solution generates the highly reactive, but short-lived, cation $^3\mathbf{2}^+$, the only fate of which is intramolecular insertion to give **3**. However, fluoroquinolones are known to insert into the distorted DNA segment bound to the gyrase active site, either by intercalating between the bases on both sides of the double helix or by replacing cytosine and forming hydrogen bonds with a guanine on the opposite strand.[20] Thus, when photoexcitation involves a molecule of **1** intercalated with DNA, the likelihood of an attack by $\mathbf{2}^+$ on a neighboring biomolecule is high. The model reaction with pyrrole in solution suggests that electrophilic attack on a DNA base could occur in that case ([Eq. (4)], compare [Eq. (3)]). Another possibility, in view of the accessible reduction potential of the quinolinyl cation, is that electron, rather than energy, transfer occurs [Eq. (5)] and causes pyrimidine dimerization.[6,21]

$$\mathbf{1} + h\nu \rightarrow {}^3\mathbf{2}^+ \quad (4a)$$

$${}^3\mathbf{2}^+ + \text{DNA base} \rightarrow \text{products} \quad (4b)$$

$$\mathbf{1} + h\nu \rightarrow {}^3\mathbf{2}^+ \quad (5a)$$

$${}^3\mathbf{2}^+ + \text{DNA base} \rightarrow \mathbf{2}^\bullet + \text{DNA base}^{\bullet+} \quad (5b)$$

$$\text{DNA base}^{\bullet+} \rightarrow \text{dimers} \quad (5c)$$

Conclusion

Fluoroquinolones, and in particular 8-fluoro derivatives such as lomefloxacin, are distinguished for their high photo-(geno)toxic potential, which must be related to their characteristic photoreaction: C–F bond heterolysis to give an aryl cation. In this work, photoproduct studies and time-resolved techniques were exploited for characterizing bimolecular reactions, and DFT and post-HF calculations were used for the first time for the detailed rationalization of the chemistry of the cation, which has proven to be particularly involved. The triplet quinolinyl cation $^3\mathbf{2}^+$ formed from $^3\mathbf{1}$ (both intermediates identified by flash photolysis) is a viable precursor of all the observed processes. Theoretical modeling reproduced intramolecular cyclization of the cation, as well as its trapping by nucleophiles (when charged or good donors), giving two different products types, either with the entering group at C_8 or, when electron transfer intervenes, at the β position in the ethyl chain.

The chemical study suggests that the genotoxic effect of **1** involves either addition of the corresponding triplet aryl cation onto a DNA base or electron-transfer-induced dimerization of the bases. More generally, the above discussion suggests that chemical studies of phototoxic drugs may concur to the understanding of their action on DNA, and possibly help to devise new models for light-activated antitumor drugs.

Experimental Section

Preparative photochemical reactions: A solution of lomefloxacin **1** (140 mg, 5×10^{-4} M) in bidistilled water (800 mL) containing the appropri-

ate amount of additive was placed in an immersion-well apparatus, stirred, and flushed with nitrogen for 30 min and then irradiated by means of a 125-W high-pressure mercury lamp at 20 °C while maintaining the nitrogen flux. Monitoring by HPLC (Hypersil ODS2, 250×4.6 mm, 5 μm, pH-3 phosphate buffer/MeCN 8:2 as eluant, flux 0.6 mL min^{-1}, λ = 275 nm) showed that the starting material was consumed after 60 min. The solution was stirred for 2 h with 2×400 mL 1% ethyl chloroformate in chloroform. The organic layers were reunited, dried, concentrated and when required treated with ethereal diazomethane. The solution was evaporated and the residue subjected to chromatography on silica gel eluting with chloroform/methanol mixtures of 98:2→95:5. The products from the photolysis of lomefloxacin were thereby isolated as the respective urethanes (in some case also methyl esters by treatment with diazomethane). The structure assignment was based on elemental analyses and spectroscopic characterization, in particular by ^{1}H, ^{13}C NMR (in $CDCl_3$, 300 MHz with TMS as internal standard), and appropriate bidimensional techniques. Key spectroscopic data of new compounds are reported below.

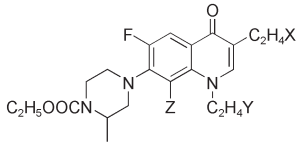

14a: X=Me, Y=H, Z=Br
b: Me H I
c: H I H
d: Me 2-furyl H

8-Bromo-1-ethyl-6-fluoro-7-[1-(3-methyl-4-ethylaminocarbonylpiperazino)]-4-quinolone-3-carboxylic acid methyl ester (14a): ^{1}H NMR (300 MHz, $CDCl_3$): δ = 1.3 (t, J = 7 Hz, 3H), 1.4 (d, J = 7 Hz, 3H), 1.5 (t, J = 7 Hz, 3H), 2.95, 3.45 (2×m, 2H), 3.15, 3.65 (2×m, 2H), 3.2, 4.0 (2×m, 2H), 3.9 (s, 1H), 4.15 (q, J = 7 Hz, 2H), 4.4 (m, 1H), 4.65 (m, 2H), 8.2 (d, J = 12 Hz, 1H), 8.75 ppm (s, 1H); ^{13}C NMR (75 MHz, $CDCl_3$): δ = 14.6 (CH_3), 15.8 (CH_3), 15.9 (CH_3), 38.9 (CH_2), 47.4 (CH), 51.6 (CH_2), 51.9 (CH_2), 52.1 (CH_2), 55,4 (CH_2), 61.5 (CH_2), 109.1 (C), 113.3 (d, J_{C-F} = 24 Hz, CH), 126.2 (C), 129.5 (C), 137.4 (C), 143.7 (C, d, J = 15 Hz), 152.5 (CH), 155.5 (C), 157.0 (d, J_{C-F} = 260 Hz, C), 166.1 (C), 172.2 ppm (C); elemental analysis calcd (%) for $C_{21}H_{25}BrFN_3O_5$ (498.34): C 50.61, H 4.97, N 9.86; found: C 50.4, H 5.0, N 9.5.

8-Iodo-1-ethyl-6-fluoro-7-[1-(3-methyl-4-ethylaminocarbonylpiperazino)]-4-quinolone-3-carboxylic acid methyl ester (14b): ^{1}H NMR (300 MHz, $CDCl_3$): δ (at 45 °C) = 1.3 (t, J = 7 Hz, 3H), 1.4 (t, J = 7 Hz, 3H), 1.5 (d, J = 7 Hz, 3H), 2.9, 3.25 (2×m, 2H), 3.1, 4.05 (2×m, 2H), 3.2, 3.8 (2×m, 2H), 3.9 (s, 3H), 4.2 (q, J = 7 Hz, 2H), 4.4 (m, 1H), 4.7 (m, 2H), 8.2 (d, J = 10 Hz, 1H), 8.8 ppm (s, 1H); ^{13}C NMR (75 MHz): δ = 14.5 (CH_3), 15.5 (CH_3), 16.8 (CH_3), 39.1 (CH_2), 47.3 (CH), 51.8 ($2CH_2$), 52.1 (CH_3), 55.1 (CH_2), 61.3 (CH_2), 91.8 (d, J_{C-F} = 18 Hz, C), 115.2 (d, J_{C-F} = 24 Hz, CH), 125.9 (C), 140.8 (C), 146.0 (d, J_{C-F} = 16 Hz, CH), 152.2 (CH), 155.4 (C), 156.4 (d, J_{C-F} = 250 Hz, C), 165.6 (C), 172.3 ppm (C); elemental analysis calcd (%) for $C_{21}H_{25}FIN_3O_5$ (545.34): C 46.25, H 4.62, N 7.71; found: C 46.5, H 4.8, N 7.7.

1-(2-Iodoethyl)-6-fluoro-7-[1-(3-methyl-4-ethylaminocarbonylpiperazino)]-4-quinolone-3-carboxylic acid methyl ester (14c): ^{1}H NMR (300 MHz, $CDCl_3$): δ = 1.3 (t, J = 7 Hz, 3H), 1.4 (d, J = 7 Hz, 3H), 3.0, 3.4 (2×m, 2H), 3.15, 3.6 (2×m, 2H), 3.5, 4.15 (2×m, 2H), 3.55 (t, J = 7 Hz, 2H), 4.2 (m, 2H), 4.5 (m, 1H), 4.65 (t, J = 7 Hz, 2H), 6.7 (d, J_{H-F} = 4 Hz, 1H), 8.0 (d, J_{H-F} = 10 Hz, 1H), 8.7 ppm (s, 1H); ^{13}C NMR (75 MHz): δ = 2.5 (CH_2), 14.5 (CH_3), 15.5 (CH_3), 38.4 (CH_2), 46.9 (CH), 49.45 (CH_2), 54.4 (CH_2), 55.9 (CH_2), 61.6 (CH_2), 103.1 (CH), 108.3 (C), 113.2 (d, J = 22 Hz, CH), 120.4 (d, J_{C-F} = 15 Hz, C), 136.6 (C), 146.6 (d, J_{C-F} = 12 Hz, C), 147.6 (CH), 153.3 (d, J_{C-F} = 250 Hz, C), 155.1 (C), 166.6 (C), 167.0 ppm (C); elemental analysis calcd (%) for $C_{20}H_{23}FIN_3O_5$ (531.32): C 45.21, H 4.36, N 7.91; found: C 45.5, H 4.0, N 8.1.

1-[2-(2-Furanyl)-ethyl]-6-fluoro-7-[1-(3-methyl-4-ethylaminocarbonylpiperazino)]-4-quinolone-3-carboxylic acid methyl ester (14d): ^{1}H NMR (300 MHz, $CDCl_3$): δ = 1.3 (t, J = 7 Hz, 3H), 1.4 (t, J = 7 Hz, 3H), 2.9, 3.35 (2×m, 2H), 3.1, 3.55 (2×m, 2H), 3.35 (m, 2H), 3.4, 4.15 (2×m, 2H), 3.8 (s, 3H), 4.2 (m, 2H), 4.4 (m, 1H), 4.45 (m, 2H), 6.0 (brs, 1H), 6.15 (brs, 1H), 6.5 (d, J_{H-F} = 7 Hz, 1H), 6.7 (brs, 1H), 7.75 (d, J_{H-F} = 13 Hz, 1H), 8.35 (s, 1H), 9.2 ppm (brs, 1H); ^{13}C NMR (75 MHz): δ = 15.1 (CH_3), 15.85 (CH_3), 28.6 (CH_2), 39.1 (CH_2), 47.5 (CH), 49.8 (CH_2), 51.9 (CH_3), 54.9 (CH_2), 55.8 (CH_2), 61.9 (CH_2), 105.1 (CH), 106.7 (CH), 108.8 (CH), 109.5 (C), 112.9 (d, J_{C-F} = 22 Hz, CH), 118.6 (CH), 121.0 (C), 123.2 (d, J_{C-F} = 6 Hz, CH), 127.8 (C), 137.2 (C), 145,5 (d, J_{C-F} = 10 Hz), 149.1 (CH), 153.0 (d, J_{C-F} = 250 Hz, C), 155.8 (C), 165.5 (C), 173.4 ppm (C); elemental analysis calcd (%) for $C_{25}H_{29}FN_4O_5$ (484.52): C 61.97, H 6.03, N 11.56; found: C 62.1, H 6.0, N 11.9.

Small-scale irradiations: Small-scale photochemical irradiation for determining the relative rate of reactions with additives were carried out on 10-mL portions of aqueous solution of **1** in serum-capped quartz tubes. These were irradiated in a merry-go-round apparatus by means of two 15-W phosphor-coated lamps (center of emission 313 nm). Deoxygenation of the solution was obtained by flushing for 30 min with argon. The experiments in the presence of halides were conducted with a total salt concentration of 0.2 M by adding the appropriate amount of $NaClO_4$. The substrate conversion and product yields were determined by HPLC (see above) on the basis of appropriate calibration curves.

Computational methods: All calculations were carried out by using the C.02 version of the Gaussian 03[22] program suite.

The geometric structures of the reactants and transition states were fully optimized both in the gas phase and in aqueous solution by using the hybrid density functional (U)B3LYP[23] with the 6-31+G(d,p) basis set. Optimization of both singlet and triplet aryl cations was also performed at the MP2/6-31+G(d,p) level of theory in the gas phase. The use of diffuse functions is mandatory for a reliable evaluation of energies in anionic systems such as **TS-8-Nu**.

The basis-set functions specifically used for Br and I atoms have been the effective core potentials (ECP) CEP/31G[24] and LANL2DZ[25] with comparable results. With these basis sets only valence electrons for Br and I atoms are treated explicitly.

Thermal contributions (δG) to free energy (ΔG) were computed from B3LYP/6-31+G(d,p) structures and harmonic frequencies by using the harmonic oscillator approximation and the standard expressions for an ideal gas in the canonical ensemble at 298.15 K and 1 atm.

The optimization of the stationary points in the solvent bulk were calculated by means of the self-consistent reaction field (SCRF) method using the PCM (polarizable continuum model)[17b] as implemented in the C.02 version of Gaussian 2003. The cavity is composed by interlocking spheres centered on non-hydrogen atoms with radii obtained by the HF parametrization by Barone known as the united atom topological model (UAHF).[27] Such a model includes the non-electrostatic terms (cavitation, dispersion and repulsion energy) in addition to the classical electrostatic contribution. We remind readers that the energies resulting from PCM computations have the status of free energies, as they take implicitly into account thermal and entropic contributions of the solvent. However, because they do not include the thermal contributions (δG) of solute molecular motions to the free energy (ΔG), gas-phase thermal contribution of solute molecular motions were added to evaluate the corresponding free energy in water (ΔGsol). UAO parametrization of the cavity has been also used and has yielded almost identical results in geometries and very similar data on energies.

Nanosecond laser flash photolysis: The laser beam (a JK-lasers Nd/YAG operated at 355 nm, pulse FWHM 20 ns) was focused on a 3 mm high and 10 mm wide rectangular area of the cell and the first 2 mm in depth were analyzed at a right angle geometry. The incident pulse energies used were $<$17 mJ cm^{-2} (5 mJ per pulse). The minimum response time of the detection system was of ca. 2 ns. The bandwidth used in the spectrokinetic measurements was typically 2 nm. The sample absorbance at 355 nm was typically 0.2 over 1 cm. Oxygen was removed by vigorously bubbling the solutions with a constant flux of N_2O. The solution, in a flow cell of 1 cm path, was renewed after few laser shots. The temperature was 295±2 K. The detector system was perturbed from 390 nm to 480 nm by the intense emission of **1**, generated by the laser excitation. These problems were minimized by using neutral density filters at the entrance slit of the monochromator and pulsing the 150 W high pressure Xe lamp at high currents (≈200 mA for 1 ms) to increase the intensity of

the analyzing light. In spite of this, transient spectra were not significant before 10–30 ns from pulse end. Acquisition of absorption signals were performed by a home made program using Asyst 3.1 (Software Technologies, Inc.).

Acknowledgements

We thank Dr. Francesco Manoli for technical support and MIUR for partial support of this work.

[1] a) S. S. Wolkenberg, D. L. Boger, *Chem. Rev.* **2002**, *102*, 2477; b) S. R. Rajski, R. M. Williams, *Chem. Rev.* **1998**, *98*, 2723; c) F. P. Gasparro, B. Liao, P. J. Foley, X. M. Wang, J. M. McNiff, *Environ. Mol. Mutagen.* **1998**, *31*, 105; d) M. Chatterjee, S. E. Rokita, *J. Am. Chem. Soc.* **1994**, *116*, 1690; e) S. N. Richter, S. Maggi, S. Colloredo-Mels, M. Palumbo, M. Freccero, *J. Am. Chem. Soc.* **2004**, *126*, 13973.

[2] L. J. Piddock, M. C. Hall, R. Wise, *Antimicrob. Agents Chemother.* **1990**, *34*, 1088.

[3] a) N. J. Traynor, M. D. Barratt, W. W. Lovell, J. Ferguson, N. K. Gibbs, *Toxicol. in Vitro* **2000**, *14*, 275; b) N. J. Neumann, A. Blotz, G. Wasinska-Kempka, M. Rosenbruch, P. Lehmann, H. J. Ahr, H. W. Vohr, *J. Photochem. Photobiol. B* **2005**, *4*, 25.

[4] a) L. Marrot, J. P. Belaidi, C. Jones, P. Perez, L. Riou, A. Sarasin, J. R. Meunier, *J. Invest. Dermatol.* **2003**, *121*, 596; b) L. Marrot, C. Agapakis-Causse, *Mutat. Res.* **2000**, *468*, 1.

[5] a) G. Klecak, F. Urbach, H. Urwyler, *J. Photochem. Photobiol. B* **1997**, *37*, 174; b) T. Itoh, H. Miyauchi-Hashimoto A. Sugihara, K. Tanaka, T. Horio, *J. Invest. Dermatol.* **2005**, *125*, 554.

[6] a) L. J. Martinez, R. H. Sik, C. Chignell, *Photochem. Photobiol.* **1998**, *67*, 399; b) N. Wagai, K. Tawara, *Arch. Toxicol.* **1992**, *66*, 392; c) L. K. Verna, D. Chen, G. Schluter, G. M. Williams, *Cell Biol. Toxicol.* **1998**, *14*, 237; d) J. E. Rosen, A. K. Prahalad, G. Schluter, D. Chen, G. M. Williams, *Photochem. Photobiol.* **1997**, *65*, 990; e) C. E. Perrone, K. C. Takahashi, G. M. Williams, *Toxicol. Sci.* **2002**, *69*, 16.

[7] a) N. J. Traynor, N. K. Gibbs, *Photochem. Photobiol.* **1999**, *70*, 957; b) S. Sauvaigo, T. Douki, F. Odin, S. Caillat, J. L. Ravanat, J. Cadet, *Photochem. Photobiol.* **2001**, *73*, 230.

[8] F. Boscà, V. Lhlaubet-Vallet, M. C. Cuquerella, J. V. Castell, M. A. Miranda, *J. Am. Chem. Soc.* **2006**, *128*, 6318.

[9] S. Monti, S. Sortino, E. Fasani, A. Albini, *Chem. Eur. J.* **2001**, *7*, 2185.

[10] a) E. Fasani, F. F. Barberis Negra, M. Mella, S. Monti, A. Albini, *J. Org. Chem.* **1999**, *64*, 5388; b) H. de Vries, G. Beijersbergen van Henegouwen, *J. Photochem. Photobiol. B* **2000**, *58*, 6.

[11] M. C. Cuquerella, M. A. Miranda, F. Boscà, *J. Phys. Chem. B* **2006**, *110*, 6441.

[12] P. J. Stang in *Divalent Carbocations* (Eds.: Z. Rappoport, P. J. Stang) Wiley, Chichester, **1997**, p. 451.

[13] M. Fagnoni, A. Albini, *Acc. Chem. Res.* **2005**, *38*, 713.

[14] Examples of intramolecular insertion into a C–H bond have been reported previously with a *o*-diazoniumdibenzylbenzamide salt (see ref. [14a]) and with *o*-propylchlorobenzene (ref. [14b]); a) T. Cohen, J. Lipowits, *J. Am. Chem. Soc.* **1964**, *86*, 2515; b) K. Hori, T. Sonoda, M. Harada, S. Yamazaki-Nishida, *Tetrahedron* **2000**, *56*, 1429.

[15] E. Fasani, M. A. Rampi, A. Albini, *J. Chem. Soc. Perkin Trans. 2* **1999**, 1901.

[16] In fact, we located an early transition structure at the B3LYP/6-31+G(d,p) level only in water, not in gas. At MP2/6-31G(d) a TS in gas had an activation energy of 3.1 kcal mol^{-1}.

[17] a) Experimental redox potential $E(\mathrm{I}^{\bullet}+\mathrm{e}\rightarrow\mathrm{I}^{-})+1.33$ V vs NHE, see: H. A. Schwarz, B. H. J. Bielski, *J. Phys. Chem.* **1986**, *90*, 1445; b) V. Barone, M. Cossi, *J. Phys. Chem. A* **1998**, *102*, 1995.

[18] H. D. Tabba, K. M. Smith, *J. Org. Chem.* **1984**, *49*, 1870.

[19] R. D. Bach, M. D. Su, E. Aldabbagh, J. L. Andres, H. B. Schlegel, *J. Am. Chem. Soc.* **1993**, *115*, 10237.

[20] a) J. Heddle, A. Maxwell, *Antimicrob. Agents Chemother.* **2002**, 1805; b) L. A. Mitscher, *Chem. Rev.* **2005**, *105*, 559; c) L. L. Shen, J. Baranowski, G. Pernet, *Biochemistry* **1989**, *28*, 3879.

[21] Guanosine is more easily oxidized than pyrrole, $E=1.29$ V vs NHE, and thymine less easily; at any rate, the process observed will depend on the closest-lying bases in the preferred intercalation; a) S. Steenken, S. V. Jovanovic, *J. Am. Chem. Soc.* **1997**, *119*, 617; b) A. Joy, A. K. Ghosh, G. B. Schuster, *J. Am. Chem. Soc.* **2006**, *128*, 5346.

[22] Gaussian 03, Revision C.02, M. J. Frisch, G. W. Trucks, H. B. Schlegel, G. E. Scuseria, M. A. Robb, J. R. Cheeseman, J. A. Montgomery, Jr., T. Vreven, K. N. Kudin, J. C. Burant, J. M. Millam, S. S. Iyengar, J. Tomasi, V. Barone, B. Mennucci, M. Cossi, G. Scalmani, N. Rega, G. A. Petersson, H. Nakatsuji, M. Hada, M. Ehara, K. Toyota, R. Fukuda, J. Hasegawa, M. Ishida, T. Nakajima, Y. Honda, O. Kitao, H. Nakai, M. Klene, X. Li, J. E. Knox, H. P. Hratchian, J. B. Cross, C. Adamo, J. Jaramillo, R. Gomperts, R. E. Stratmann, O. Yazyev, A. J. Austin, R. Cammi, C. Pomelli, J. W. Ochterski, P. Y. Ayala, K. Morokuma, G. A. Voth, P. Salvador, J. J. Dannenberg, V. G. Zakrzewski, S. Dapprich, A. D. Daniels, M. C. Strain, O. Farkas, D. K. Malick, A. D. Rabuck, K. Raghavachari, J. B. Foresman, J. V. Ortiz, Q. Cui, A. G. Baboul, S. Clifford, J. Cioslowski, B. B. Stefanov, G. Liu, A. Liashenko, P. Piskorz, I. Komaromi, R. L. Martin, D. J. Fox, T. Keith, M. A. Al-Laham, C. Y. Peng, A. Nanayakkara, M. Challacombe, P. M. W. Gill, B. Johnson, W. Chen, M. W. Wong, C. Gonzalez, J. A. Pople, Gaussian, Inc., Pittsburgh PA, **2003**.

[23] a) A. D. Becke, *J. Chem. Phys.* **1993**, *98*, 1372; b) H. L. Schmider, A. D. Becke, *J. Chem. Phys.* **1998**, *108*, 9624.

[24] a) W. Stevens, H. Basch, J. Krauss, *J. Chem. Phys.* **1984**, *81*, 6026; b) T. R. Cundary, W. Stevens, *J. Chem. Phys.* **1993**, *98*, 5555.

[25] a) W. R. Wadt, P. J. Hay, *J. Chem. Phys.* **1985**, *82*, 270; b) P. J. Hay, W. R. Wadt, *J. Chem. Phys.* **1985**, *82*, 284; c) W. R. Wadt, P. J. Hay, *J. Chem. Phys.* **1985**, *82*, 299.

[26] For a more comprehensive treatment of solvation models, see: C. J. Cramer, D. G. Truhlar, *Chem. Rev.* **1999**, *99*, 2161.

[27] V. Barone, M. Cossi, J. Tomasi, *J. Chem. Phys.* **1997**, *107*, 3210.

Received: July 17, 2007
Published online: October 17, 2007

